Lattice-Boltzmann simulations of the dynamics of polymer solutions in periodic and confined geometries

O. Berk Usta,[a] Anthony J. C. Ladd,[b] and Jason E. Butler[c]
Department of Chemical Engineering, University of Florida, Gainesville, Florida 32611

(Received 21 October 2004; accepted 7 December 2004; published online 24 February 2005)

A numerical method to simulate the dynamics of polymer solutions in confined geometries has been implemented and tested. The method combines a fluctuating lattice-Boltzmann model of the solvent [Ladd, Phys. Rev. Lett. **70**, 1339 (1993)] with a point-particle model of the polymer chains. A friction term couples the monomers to the fluid [Ahlrichs and Dünweg, J. Chem. Phys. **111**, 8225 (1999)], providing both the hydrodynamic interactions between the monomers and the correlated random forces. The coupled equations for particles and fluid are solved on an inertial time scale, which proves to be surprisingly simple and efficient, avoiding the costly linear algebra associated with Brownian dynamics. Complex confined geometries can be represented by a straightforward mapping of the boundary surfaces onto a regular three-dimensional grid. The hydrodynamic interactions between monomers are shown to compare well with solutions of the Stokes equations down to distances of the order of the grid spacing. Numerical results are presented for the radius of gyration, end-to-end distance, and diffusion coefficient of an isolated polymer chain, ranging from 16 to 1024 monomers in length. The simulations are in excellent agreement with renormalization group calculations for an excluded volume chain. We show that hydrodynamic interactions in large polymers can be systematically coarse-grained to substantially reduce the computational cost of the simulation. Finally, we examine the effects of confinement and flow on the polymer distribution and diffusion constant in a narrow channel. Our results support the qualitative conclusions of recent Brownian dynamics simulations of confined polymers [Jendrejack *et al.*, J. Chem. Phys. **119**, 1165 (2003) and Jendrejack *et al.*, J. Chem. Phys. **120**, 2513 (2004)]. © *2005 American Institute of Physics*. [DOI: 10.1063/1.1854151]

I. INTRODUCTION

Numerical simulations of the dynamics of polymer solutions are computationally demanding because of the wide range of length scales and time scales in the system. Hydrodynamic interactions are necessary to obtain even qualitatively correct scaling laws, but Brownian dynamics, the standard simulation technique for polymer solutions, then becomes computationally expensive. The time to calculate a single step for a chain of N segments scales as N^3 when hydrodynamic interactions are included, with the computational cost dominated by the factorization of the mobility matrix. To calculate average properties, the simulations must be performed over many Zimm relaxation times, $t_Z \sim \eta b^3 N^{3\nu}/T$; here η is the solvent viscosity, b is the segment length, T is the temperature, and the excluded-volume exponent $\nu \approx 0.6$. The number of time steps required for comparable statistical accuracy in the diffusivity or other average property is therefore proportional to $N^{3\nu}$. Thus, the overall computation time for a dynamical simulation scales as $N^{4.8}$, although an approximate factorization of the mobility matrix[1,2] reduces this to $N^{3.8}$, but with possible loss of positive definiteness.[2] Still, the maximum chain length that can be studied by Brownian dynamics is of the order of 100 monomers,[2–6] which is not always sufficient to determine accurate rheological properties of flexible polymers.[7,8] In a semidilute solution of N_c chains, the computational cost of Brownian dynamics increases further, in proportion to N_c^2 or N_c^3 depending on the method of factorization.

In addition to the unfortunate scaling of the computational cost, Brownian dynamics is not easily extended to include external boundaries and flow fields. No-slip boundaries require a complicated Green's function even for channel flows,[2] while more involved geometries can only be handled by finite-element or boundary-element methods. Brownian dynamics has no straightforward way of including any external flow field beyond a simple linear shear flow. More complex flows require a coupled calculation of the evolution of the fluid velocity field with the dynamics of the particle chains. Even the great advantage of Brownian dynamics, which is the capability to solve directly for the dynamics on the diffusive time scale, is negated by the very small time step that is necessary to integrate the stochastic equations, typically $10^{-5} t_Z$ for moderate length chains ($N \sim 100$). We will see that comparable time steps can be used in inertial simulations.

The computational method presented here is based on a fluctuating lattice-Boltzmann model of the fluid phase,[9,10] which includes thermally driven fluctuations in the fluid velocity field via random fluctuations added to the stress tensor. The key difference with Brownian dynamics is that these

[a]Electronic mail: ousta@che.ufl.edu
[b]Electronic mail: ladd@che.ufl.edu; URL: http://ladd.che.ufl.edu/
[c]Electronic mail: butler@che.ufl.edu

random fluctuations are local in space and time, avoiding any factorization of the covariance matrix. Instead, initially uncorrelated fluctuations develop in space and time by viscous diffusion of momentum, giving rise to hydrodynamic correlations at sufficiently large spatial and temporal scales. Numerical simulations have shown that the dissipative and fluctuating hydrodynamic interactions between finite-size particles can be reproduced quantitatively.[11] Computationally, the lattice-Boltzmann method is inherently and straightforwardly parallelizable, enabling large simulations to be spread across a cluster of processors with a relatively low network bandwidth.

The lattice-Boltzmann method has been used for a wide variety of complex flows, including suspensions of colloidal[12,13] and noncolloidal[14–16] particles, and porous media.[17–19] Since the fluid equations are solved on a grid, external boundaries and imposed flow fields can be included at no additional computational cost. However, suspended solid particles occupy a substantial fluid volume, typically of the order of 100 grid points, and interact with the fluid through boundary nodes distributed on the particle surface. Since the computation time of the method is proportional to the fluid volume, the suspension model is unnecessarily expensive for polymer solutions, where the monomers can be modeled as point forces coupled to the fluid by a friction coefficient, ξ. Ahlrichs and Dünweg integrated this frictional coupling into the fluctuating lattice-Boltzmann model and investigated the static and dynamical scaling laws of individual polymers and semidilute solutions.[20,21]

In this paper we report extensive tests of this method for individual monomers, as well as applications to the diffusion of polymer chains in periodic and confined geometries. We show that the Oseen limit of the dissipative and fluctuating hydrodynamic interactions between two monomers is obtained for separations larger than Δx, the grid spacing of the lattice-Boltzmann model. We also show that the radius of gyration, end-to-end distance, and diffusion coefficient of a flexible excluded volume chain agree quantitatively with renormalization group calculations[22] for chains up to 1024 monomers. A coarse-graining of the hydrodynamic interactions has been investigated, which suggests the possibility of a considerable speed up in the computation for large chains. Despite the extra inertial time scale, our simulations use time steps that are comparable to Brownian dynamics, and therefore achieve a more favorable scaling of the computational time with chain length. We briefly investigate the effects of confinement and flow on the polymer distribution in a two-dimensional channel.

II. SIMULATION METHOD

The simulation method couples a standard model for a flexible polymer with a lattice-Boltzmann model of the surrounding solvent, which includes the thermal fluctuations in the fluid velocity field. The polymer is modeled as a chain of interacting mass points, coupled together by springs with a rest length b. Other models, such as a wormlike chain,[23] can well be equally implemented. The fluid exerts a frictional drag force on each monomer in the chain, based on the difference between the velocity of the monomer and the local velocity of the fluid. The force exerted by the monomers is redistributed back into the fluid; in other words there is a two-way coupling of the momentum transfer. The method provides a straightforward and computationally efficient alternative to Brownian Dynamics, but incorporates the same level of description of the hydrodynamic and thermodynamic forces, although they are simulated on the inertial rather than the diffusive time scale.

A. Lattice-Boltzmann equation

The fundamental quantity in the lattice-Boltzmann model is the discretized one-particle velocity distribution function $n_i(\mathbf{r},t)$, which describes the mass density of particles with velocity $\mathbf{c}_i$, at a particular node of the lattice $\mathbf{r}$, at a discrete time t. The hydrodynamic fields, mass density ρ, momentum density $\mathbf{j}=\rho\mathbf{u}$, and momentum flux $\mathbf{\Pi}$, are moments of this velocity distribution:

$$\rho = \Sigma_i n_i, \quad \mathbf{j} = \Sigma_i n_i \mathbf{c}_i, \quad \mathbf{\Pi} = \Sigma_i n_i \mathbf{c}_i \mathbf{c}_i. \tag{1}$$

The time evolution of $n_i(\mathbf{r},t)$ is described by a discrete analogue of the Boltzmann equation,[24]

$$n_i(\mathbf{r} + \mathbf{c}_i \Delta t, t + \Delta t) = n_i(\mathbf{r},t) + \Delta_i[\mathbf{n}(\mathbf{r},t)], \tag{2}$$

where Δ_i is the change in n_i due to instantaneous collisions at the lattice nodes and Δt is the time step. Somewhat surprisingly, this simple evolution equation is second-order accurate in space and time. The numerical diffusion that usually accompanies a low-order grid-based method is eliminated by the relationship between the eigenvalues of the linearized collision operator and the fluid viscosity.

The standard 19 velocity model comprises stationary particles and the 18 velocities corresponding to the [100] and [110] directions of a simple cubic lattice. The population density associated with each velocity has a weight a^{c_i} that describes the fraction of particles with velocity $\mathbf{c}_i$ in a system at rest; these weights depend only on the speed c_i and are normalized so that $\Sigma_i a^{c_i}=1$. The optimum choice of weights for this model is

$$a^0 = \tfrac{1}{3}, \quad a^1 = \tfrac{1}{18}, \quad a^{\sqrt{2}} = \tfrac{1}{36}. \tag{3}$$

In these simulations we use a three-parameter collision operator, allowing for separate relaxation of the five shear modes, one bulk mode, and nine kinetic modes. The post-collision distribution $n_i^\star = n_i + \Delta_i$ is written as

$$n_i^\star = a^{c_i}\left(\rho + \frac{\mathbf{j}\cdot\mathbf{c}_i}{c_s^2} + \frac{(\rho\mathbf{uu} + \mathbf{\Pi}^{\mathrm{neq},\star}):(\mathbf{c}_i\mathbf{c}_i - c_s^2\mathbf{1})}{2c_s^4}\right), \tag{4}$$

where the sound speed $c_s=\Delta x/\sqrt{3}\Delta t$, Δx is the spacing between neighboring fluid nodes, and Δt is the time step. In suspensions of moving particles, the nonlinear $\rho\mathbf{uu}$ term in Eq. (4) should be retained, since it maintains Galilean invariance and prevents an artificial cross-stream drift. Empirically, we have found that the domain of validity of Stokes flow is considerably larger with the nonlinear term in place.

The non-equilibrium momentum flux $\mathbf{\Pi}^{\mathrm{neq}}=\Sigma_i n_i^{\mathrm{neq}}\mathbf{c}_i\mathbf{c}_i$ relaxes due to collisions at the lattice nodes,

$$\mathbf{\Pi}^{\mathrm{neq},\star} = (1+\lambda)\overline{\mathbf{\Pi}}^{\mathrm{neq}} + \tfrac{1}{3}(1+\lambda_v)(\mathbf{\Pi}^{\mathrm{neq}}:\mathbf{1})\mathbf{1}, \tag{5}$$

where $\mathbf{\Pi}^{\mathrm{neq}} = \mathbf{\Pi} - \mathbf{\Pi}^{\mathrm{eq}}$, $\mathbf{\Pi}^{\mathrm{eq}} = \rho c_s^2 + \rho\mathbf{uu}$ is the equilibrium momentum flux, and $\overline{\mathbf{\Pi}}^{\mathrm{neq}}$ indicates the traceless part of $\mathbf{\Pi}^{\mathrm{neq}}$. The parameters λ and λ_v are eigenvalues of the linearized collision operator and are related to the fluid shear and bulk viscosities:

$$\eta = -\rho c_s^2 \Delta t\left(\frac{1}{\lambda}+\frac{1}{2}\right), \quad \eta_v = -\frac{2\rho c_s^2}{3}\Delta t\left(\frac{1}{\lambda_v}+\frac{1}{2}\right). \tag{6}$$

The factor of $1/2$ serves to correct for numerical diffusion, so that viscous momentum diffuses at the expected speed for the given viscosity.

In the presence of an externally imposed force density $\mathbf{f}$, for example a pressure gradient or a gravitational field, the time evolution of the lattice-Boltzmann model includes an additional contribution $f_i(\mathbf{r},t)$,

$$n_i(\mathbf{r}+\mathbf{c}_i\Delta t, t+\Delta t) = n_i^{\star}(\mathbf{r},t) + f_i(\mathbf{r},t). \tag{7}$$

This forcing term can also be expanded in a power series in the velocity,

$$f_i = a^{c_i}\left[\frac{\mathbf{f}\cdot\mathbf{c}_i}{c_s^2} + \frac{(\mathbf{uf}+\mathbf{fu}):(\mathbf{c}_i\mathbf{c}_i - c_s^2\mathbf{1})}{2c_s^4}\right]\Delta t. \tag{8}$$

More accurate solutions to the velocity field are obtained if it includes a portion of the momentum added to each node,[10]

$$\mathbf{j}' = \rho\mathbf{u}' = \sum_i n_i\mathbf{c}_i + \tfrac{1}{2}\mathbf{f}\Delta t. \tag{9}$$

The macrodynamical behavior arising from the lattice-Boltzmann equation can be found from a multiscale analysis,[24] using an expansion parameter ϵ, defined as the ratio of the lattice spacing to a characteristic macroscopic length; the hydrodynamic limit corresponds to $\epsilon \ll 1$. It can be shown that the lattice-Boltzmann equation reproduces the Navier–Stokes equations with corrections that are of the order u^2 and ϵ^2. Thus, at sufficiently low Mach numbers, the method is second-order accurate in space, with relative errors proportional to Δx^2. It is also second-order accurate in time if the viscosities are defined according to Eq. (6).

B. Fluctuations

The lattice-Boltzmann model can be extended to include thermal fluctuations, which lead to Brownian motion of colloidal particles and polymers. The fluctuating lattice-Boltzmann model[9,12] incorporates a random component into the momentum flux during the collision process [cf. Eq. (5)]:

$$\mathbf{\Pi}^{\mathrm{neq},\star} = (1+\lambda)\overline{\mathbf{\Pi}}^{\mathrm{neq}} + \tfrac{1}{3}(1+\lambda_v)(\mathbf{\Pi}^{\mathrm{neq}}:\mathbf{1})\mathbf{1} + \mathbf{\Pi}^{f},$$

$$\mathbf{\Pi}^{f} = \zeta\overline{\mathbf{R}} + \zeta_v R_v\mathbf{1}, \tag{10}$$

where R_v is a random variable with zero mean and unit variance, and $\mathbf{R}$ is a symmetric matrix of random variables of zero mean. The off-diagonal elements of $\mathbf{R}$ have a variance of 1, while the diagonal elements have a variance of 2. In this particular implementation, six random numbers are required to generate the components of the symmetric matrix $\mathbf{R}$, together with the constraint that $\overline{\mathbf{R}}$ is traceless. Random numbers spanning a finite space are advantageous since the change in any one step is then limited. We use integer random numbers $[-2,-1,0,1,2]$ with weights $[1/12,1/6,1/2,1/6,1/12]$ to obtain a unit variance and second-order accuracy in time.

An analogy with fluctuating hydrodynamics[25] suggests that

$$\zeta = \left(\frac{2T\eta}{\Delta x^3\Delta t}\right)^{1/2}, \quad \zeta_v = \left(\frac{2T\eta_v}{\Delta x^3\Delta t}\right)^{1/2}, \tag{11}$$

where T is the thermal energy in units of $m_0\Delta x^2/\Delta t^2$, and $m_0 = \rho\Delta x^3/36$ is taken to be the rest mass of an individual population density. However, detailed calculations show that discrete lattice artifacts again modify the results for continuous fluids.[9,10] The correct coefficients, determined by relating the decay of long wavelength stress fluctuations to the viscosity of the lattice-Boltzmann fluid are[9,10]

$$\zeta = \left(\frac{2T\eta\lambda^2}{\Delta x^3\Delta t}\right)^{1/2}, \quad \zeta_v = \left(\frac{2T\eta_v\lambda_v^2}{\Delta x^3\Delta t}\right)^{1/2}. \tag{12}$$

There is an additional multiplicative factor of $\sqrt{\lambda^2}$ [cf. Eq. (11)], but for $\lambda=\lambda_v=-1$, an exact correspondence with the fluctuation-dissipation relation for continuous systems is obtained. However the discrete version [Eq. (12)] can also be applied to systems where the viscous eigenvalues are not equal to -1.[9] This may be advantageous in problems where a time-scale separation is required between hydrodynamic and kinetic modes.

C. Polymer-fluid coupling

The polymer chain is represented by a bead-spring model with an equilibrium bond length b between neighboring beads. The spring stiffness, $\kappa = 30T/b^2$, was chosen so that the fluctuations in bond length, $\langle(r-b)^2\rangle^{1/2} = b/\sqrt{30}$, were small in comparison with the radius of gyration of the chain, R_g. A hard-sphere excluded-volume interaction between the monomers was included, with collision diameter $b/2$. Other excluded volume and intrachain potentials could be equally well used.

The equations of motion for the monomers are written in inertial form,

$$m\frac{d^2\mathbf{X}_i}{dt^2} = -\nabla_i\Phi(\mathbf{X}^N) + \mathbf{F}_i^f, \tag{13}$$

where Φ is the total potential energy, and $\mathbf{F}_i^f$ is the hydrodynamic force exerted on bead i by the fluid. The Brownian dynamics algorithm is derived from Eq. (13) by neglecting the inertial term and integrating the random component of the hydrodynamic force over the duration of the time step.[26] In this paper evidence will be presented to support our contention that it is more efficient to integrate Eq. (13) directly. The large time-scale separation between the dynamics of the polymer and the individual monomers allows time for the hydrodynamic interactions to reach a quasisteady state, without imposing this condition at each and every time step. We will show that both inertial and diffusive simulations can use

similar time steps, of the order of the monomer diffusion time. This allows for orders of magnitude savings in computation time by keeping the interactions local in space. We note that the lattice-Boltzmann model is just one possible framework for such calculations, which could also be carried out within a fluctuating finite-difference or finite-element simulation of the fluid.

The hydrodynamic interactions between the beads are determined by coupling them individually to the fluctuating lattice-Boltzmann model, from which the mesoscopic equations for a fluid with thermal fluctuations can be derived.[10] The coupling between the beads and the fluid is derived from a frictional force based on the difference in velocity between the bead, $\mathbf{U}$, and the surrounding fluid, $\mathbf{u}(\mathbf{r},t)$,[20]

$$\mathbf{F}^f = -\xi_0[\mathbf{U}(t) - \mathbf{u}(\mathbf{X},t)] + \mathbf{F}^r. \tag{14}$$

The random force $\mathbf{F}^r$ is introduced to balance the additional dissipation caused by using a frictional coupling instead of a no-slip boundary condition on the bead surfaces.[20] Since the fluid satisfies its own fluctuation-dissipation relation, $\mathbf{F}^r$ has a local covariance matrix

$$\langle \mathbf{F}^r(t)\mathbf{F}^r(t')\rangle = 2T\xi_0\delta(t-t')\mathbf{1}. \tag{15}$$

Hydrodynamic interactions between the beads are transmitted through the fluid via correlated fluctuations in the fluid velocity field, which develop over the inertial time scale, $\rho r^2/\eta$, where r is the separation between beads.

The point-particle approach leads to an Oseen interaction between individual monomers as will be shown numerically in Sec. III B. The time scale for hydrodynamic interactions to develop, $\rho R_g^2/\eta$, must be much shorter than the diffusion time for the polymer, R_g^2/D. In other words, viscous momentum must diffuse considerably faster than the time scale for appreciable changes in polymer configuration. This scale separation is characterized by the Schmidt number $Sc = \eta/\rho D$, which for the temperatures and bond lengths used in the simulations is in the range $3N^{\nu}-60N^{\nu}$. This scale separation is larger and more easily controlled than in dissipative particle dynamics simulations,[27] and the effect of variations in Schmidt number is usually small. The Euler method was used to integrate the equations of motion of the monomers, with a time step that was typically $1/100$ of the monomer diffusion time. When necessary, the thermodynamic forces were integrated with a smaller time step than the hydrodynamic forces to maintain stability. A hard-sphere molecular dynamics code was used at each step to detect collisions between pairs of monomers.

Since the monomers move continuously over the grid, while the velocity field is evaluated at a discrete set of points, we employ a trilinear interpolation to evaluate $\mathbf{u}(\mathbf{X},t)$, using the fluid velocities at the nodes of the cube surrounding the monomer.[20] After calculating the weights, w_i, for each of the nodes, the mass density, ρ, and the momentum density $\rho\mathbf{u}$ are interpolated to determine the velocity field at the bead location $\mathbf{X}$,

$$\mathbf{u}(\mathbf{X},t) = \frac{\Sigma_i w_i \rho_i \mathbf{u}_i}{\Sigma_i w_i \rho_i}. \tag{16}$$

To conserve momentum, the accumulated force exerted by the bead on the fluid is distributed to the surrounding nodes with the same weight function. Trilinear interpolation is computationally efficient and works satisfactorily, as demonstrated by numerical tests. However, there are discontinuities in the spatial derivative of the velocity field at the cell boundaries, which we have found can be greatly reduced by using second order interpolation. Nevertheless, the increased accuracy does not clearly justify the additional computational cost of employing a higher order interpolation. Consequently, the results in this paper use linear interpolation, though higher order interpolation schemes will be considered in future work.

D. Confined geometries

To simulate confined polymer solutions, the lattice-Boltzmann model must be modified to incorporate the boundary conditions imposed on the fluid by the solid surfaces. Stationary solid objects are described by the "bounce-back" collision rule,[24] in which incoming fluid particles are reflected back towards the nodes from which they originated. Surface forces are then calculated from the momentum transfer at each boundary node and summed to give the total force on the boundary.[9] A planar boundary is constructed from an array of boundary nodes, which are located at the midpoints of lines crossing from the last plane of fluid nodes to the lattice positions in the solid. The infrequent collisions between monomers and the confining boundaries are detected by the hard-sphere algorithm. The bounce-back rule can be modified for a moving wall, for example a planar shear flow, by altering the fluid populations reflected from the wall.[9]

III. RESULTS

In this section we summarize the results of our simulations of polymer chains in periodic and confined geometries. We begin with detailed tests of the numerical method, validating the code for both dissipative and fluctuating hydrodynamic interactions. Next we calculate the diffusion coefficient for single chains in a periodic cell, using well established finite-size corrections to estimate the diffusion coefficient at infinite dilution for chains up to 1024 monomers. Finally, we calculate the effects of confinement on the diffusion coefficient, and investigate how the polymer distribution is modified by an imposed flow field.

A. Fluctuation-dissipation

The fluctuation-dissipation theorem implies that the diffusion coefficient of an isolated monomer $D_m = T/\xi_0$, where the temperature, T, is related to the variance of the random stresses in the fluid [Eq. (12)] and ξ_0 is the monomer friction. However, as Ahlrichs and Dünweg[20] originally indicated, the diffusion coefficient of an isolated point particle is not precisely proportional to the inverse of the friction coefficient, but is offset by a constant value that is independent of the input friction ξ_0,

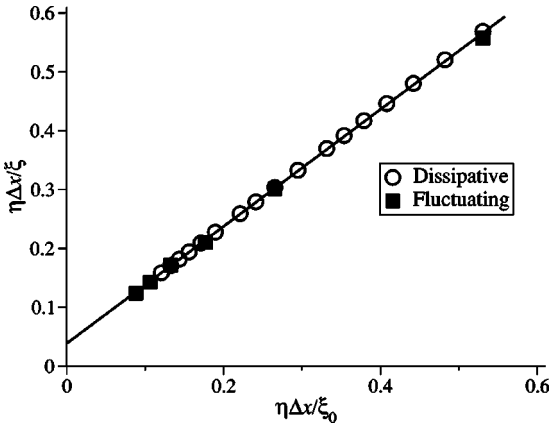

FIG. 1. Relation between the effective friction coefficient ξ and the input friction ξ_0 [Eq. (14)]. The effective friction coefficient has been obtained from the drag force on a single monomer (circles) and the diffusion of the monomer in a thermally fluctuating fluid (squares). The slope of the line is unity, indicating a constant offset between ξ^{-1} and ξ_0^{-1}. The unit cell size $L=20\Delta x$.

$$\frac{D_m}{T} = \frac{1}{\xi_0} + \frac{g}{\eta\Delta x}. \tag{17}$$

We therefore attempted to verify the Stokes–Einstein relation for a single monomer, by calculating the velocity of a monomer under an external body force as well as the diffusivity of the monomer due to thermal fluctuations in the fluid. Figure 1 summarizes the most important finding, namely that the friction-coefficient determined from the mean-square displacement of the monomer at finite temperatures, $\xi^{-1}=D_m/T$, matches the friction coefficient determined from the drag force, $F_d=-\xi U$.

Figure 1 also shows that there is a constant offset between the effective friction ξ, measured from the drag force or diffusion coefficient, and the input friction coefficient ξ_0 [Eq. (14)]. In essence, there is a renormalization of the friction coefficient by the flow field induced by the moving particle. A point force **F** applied at the origin of a continuum fluid creates a velocity field,

$$\mathbf{u}(\mathbf{r}) = \frac{1+\mathbf{rr}/r^2}{8\pi\eta r}\cdot\mathbf{F}, \tag{18}$$

that is singular at the origin. However, the discrete nature of the lattice-Boltzmann velocity field leads instead to a finite result,

$$\mathbf{u}(0) = \frac{\mathbf{F}g}{\eta\Delta x}, \tag{19}$$

where g is a numerical constant. A steady-state force balance between the imposed force **F** and the particle velocity,

$$\mathbf{F} = -\mathbf{F}_d = \xi_0[\mathbf{U}-\mathbf{u}(0)] = \xi\mathbf{U}, \tag{20}$$

leads directly to Eq. (17). Further tests verify that the parameter g is independent of solvent viscosity, confirming the relation given in Eq. (17). However, g does depend weakly on system size as shown in Fig. 2, but not on the input friction, ξ_0. The offset, g, is easily calculated for any cell geometry, using a measurement of the fluid velocity at the origin of a point force together with Eq. (19).

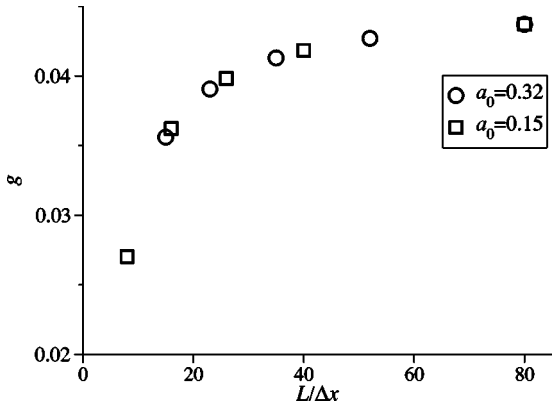

FIG. 2. Offset between ξ^{-1} and ξ_0^{-1} as a function of system volume. The variation in the dimensionless mobility g [Eq. (17)] is shown for a cubic cell of length, L. Results are shown for input hydrodynamic radii $a_0=0.32$ (circles) and $a_0=0.15$ (squares). The monomer friction $\xi_0=6\pi\eta a_0$.

When the effective size of the monomer is small compared to the grid spacing (weak friction), $\eta\Delta x/\xi \gg 1$ and the effect of the lattice renormalization is small. In this case the diffusivity is controlled by the input particle radius, $D_m/T \rightarrow 1/6\pi\eta a_0$. The opposite limit, where the particle is large compared to the grid spacing, violates the underlying assumption of the point-particle model. However, even here the diffusivity is finite but controlled by the grid spacing, $D_m/T \rightarrow g/\eta\Delta x$. In these numerical simulations the lattice contribution to the diffusivity is of the order of 25%.

The fluctuation-dissipation theorem for a discrete model does not necessarily imply equipartition of energy, as is the case for a continuous system described by the classical Langevin equation. The data in Fig. 3 show that the mean kinetic energy of a single monomer in a thermally fluctuating fluid varies between 1% and 10% from equipartition. The results can be understood by analyzing the Langevin equation for a single particle with constant friction,

$$m\dot{U} = -\xi U + F_r, \tag{21}$$

where the random force, F_r, has a variance $\langle F_r(t)F_r(t')\rangle = 2T\xi\delta(t-t')$. Solving this equation leads to the well known results $m\langle U^2\rangle = T$ and $D=T/\xi$.

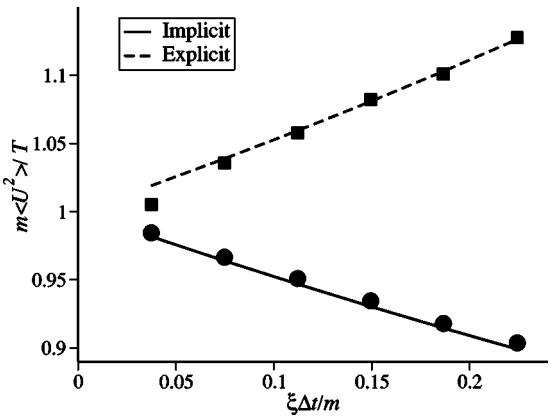

FIG. 3. Mean kinetic energy of a single monomer as a function of the dimensionless frictional coupling, $\xi\Delta t/m$. The calculated kinetic energy for implicit (circles) and explicit (squares) updates is compared with the model described in the Appendix (lines).

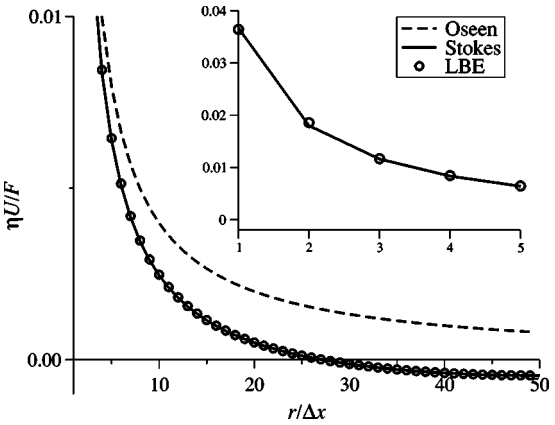

FIG. 4. Velocity due to a point force. The velocity component parallel to the direction of the force, $v_x(r,0,0)$, is plotted as a function of distance from the force. Results are shown for the Oseen flow field (dashed), the Stokes flow field in a periodic cell of length $100\Delta x$ (solid line), and lattice-Boltzmann simulations (circles) in the same size cell.

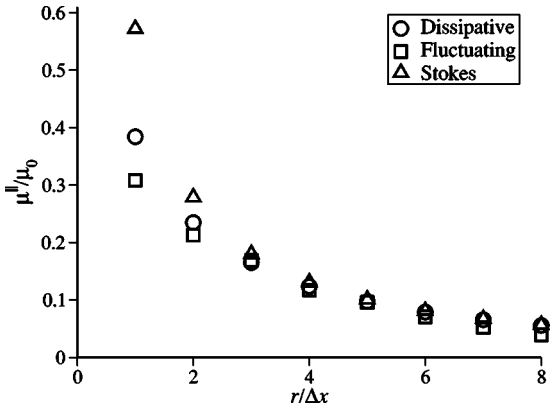

FIG. 5. Comparison of the parallel component of the two particle mobility tensor, $\mu_{12}^{\parallel}$. Results obtained by dissipative [Eq. (26), circles] and fluctuating [Eq. (27), squares] simulations are compared with an independent solution of the periodic Stokes equations [Eq. (25), triangles].

A numerical integration of this equation can be accomplished by discretization in time,

$$U(t+\Delta t) = U(t) - \Omega U(t) + \Delta U(t), \tag{22}$$

or

$$U(t+\Delta t) = U(t) - \Omega U(t+\Delta t) + \Delta U(t), \tag{23}$$

where $\Omega = \xi \Delta t/m$ and $\langle (\Delta U)^2 \rangle = 2T\Omega/m$. Equation (22) corresponds to a first-order explicit integration of Eq. (21), while Eq. (23) corresponds to an implicit integration. In the Appendix, we show that this choice of random force, derived directly from the continuous case, still satisfies the Stokes–Einstein relation $D=T/\xi$, regardless of the integration method, but classical equipartition of energy is modified,

$$m\langle U^2 \rangle = \frac{T}{1 \pm \Omega/2}; \tag{24}$$

explicit integration leads to the minus sign in the denominator of Eq. (24), while implicit integration leads to the plus sign. Figure 3 shows that this simple model accounts for the kinetic energy measured in the simulations, although here the fluctuations in particle velocity are largely driven by the fluid. The long-time dynamics of the polymer are controlled by the diffusion of the monomers, and the absence of equipartition at short times will not affect these results. We note that equipartition can be recovered by using a weaker frictional coupling or a larger particle mass, but this is not necessary for accurate results on the diffusive time scale. Therefore the Brownian relaxation time, Ω^{-1}, does not have to be large.

B. Hydrodynamic interactions

The computational method described in Sec. II provides an accurate solution for the flow-field around a point force, as can be seen in Fig. 4 where a section of the fluid velocity field is shown for a periodic cell of length $L=100\Delta x$. This example is typical of the method, which quantitatively describes the flow field on distances larger than a single grid spacing, Δx. There is a significant difference at large distances between the Oseen field for an infinite system (dashed line) and Stokes flow in a periodic cell (solid line), which was calculated from the Fourier representation,[28]

$$\mathbf{u}(\mathbf{r}) = \frac{1}{V} \sum_{\mathbf{k} \neq 0} \frac{e^{i\mathbf{k}\cdot\mathbf{r}}(\mathbf{1} - \mathbf{k}\mathbf{k}/k^2)}{\eta k^2} \cdot \mathbf{F}. \tag{25}$$

The hydrodynamic interactions between a pair of monomers have been calculated from both the dissipative response to an external force and the correlations between particle velocities in a fluctuating fluid. The pair mobility $\boldsymbol{\mu}_{ij}$ is defined in terms of the velocity induced on one particle by a force on the other,

$$\mathbf{U}_i = \boldsymbol{\mu}_{ij} \cdot \mathbf{F}_j \tag{26}$$

and also from the autocorrelation function of the particle velocity in a fluctuating fluid,

$$\boldsymbol{\mu}_{ij} = \frac{1}{T} \int_0^\infty \langle \mathbf{U}_i(t) \mathbf{U}_j(0) \rangle dt. \tag{27}$$

The linearity of Stokes flow allows us to simplify the analysis by keeping the particles fixed in place during the course of the simulation, even though the particle velocities are nonzero.

The single-particle mobility was found to be unaffected by the presence of a neighboring particle, as would be expected for point forces. The pair mobility, which can be decomposed into components parallel ($\mu^{\parallel}$) and perpendicular ($\mu^{\perp}$) to the separation vector, is shown in Figs. 5 and 6. The results for dissipative and fluctuating calculations of the mobility agree with one another and with an exact Stokes flow calculation in the same periodic geometry, Eq. (25), down to separations of the order of Δx. The discrepancies largely reflect errors in interpolating the flow field to off-lattice locations; the results shown in Fig. 4 were evaluated at the lattice nodes and are much closer to the Stokes flow result at small distances. Improved interpolation should lead to more accurate values of the mobility of closely spaced monomers.

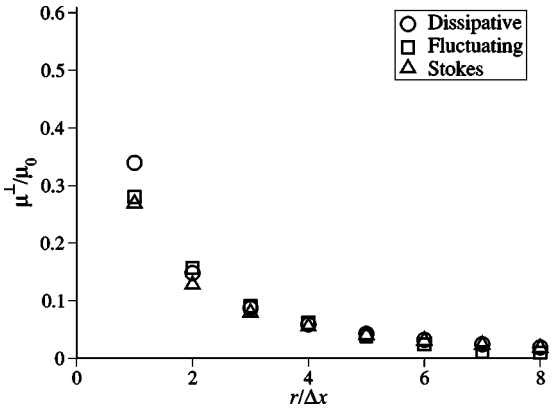

FIG. 6. Comparison of the perpendicular component of the two particle mobility tensor, $\mu_{12}^{\perp}$. Results obtained by dissipative [Eq. (26), circles] and fluctuating [Eq. (27), squares] simulations are compared with an independent solution of the periodic Stokes equations [Eq. (25), triangles].

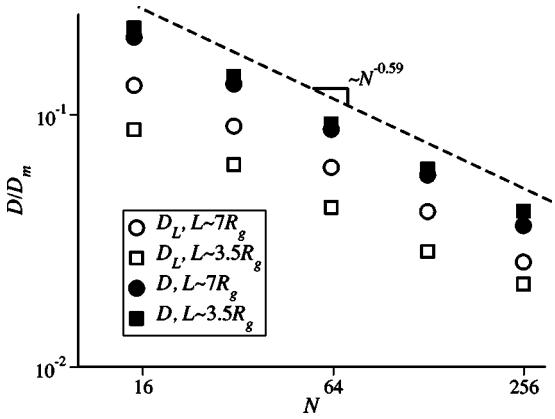

FIG. 8. Center of mass diffusion coefficient as a function of chain length in different size cells. The diffusion coefficients are normalized by the monomer diffusion coefficient, $D_m = T/\xi$, and are shown for periodic systems with lengths $L \sim 3.5R_g$ and $L \sim 7R_g$. In all cases the mean separation between the monomers $b = \Delta x$ and the temperature $T = 0.1$. Results are shown for the raw diffusion coefficient (open symbols), as well as the corrected values (filled symbols).

C. Diffusion of an isolated polymer

We have simulated the Brownian motion of individual polymers over a wide range of chain lengths, from $N = 16$ monomers to $N = 1024$. As demonstrated in the previous sections, the accuracy of the hydrodynamic interactions depends on the separation between adjacent monomers, b, in comparison to the grid spacing of the lattice-Boltzmann model, Δx. Consequently, three different values of b were used to calculate the equilibrium and nonequilibrium properties of the model polymer chain; $b = 2\Delta x$, $b = \Delta x$ as used by Ahlrichs and Dünweg,[20] and $b = 0.5\Delta x$. The monomer friction and excluded volume were also scaled in proportion to b. The computational time scales as b^6, taking into account both the change in number of grid points ($\propto b^3$) and the change in Zimm time ($\propto b^3$). The simulations were run for at least 20 Zimm times, which was sufficient to reduce the statistical errors in the diffusion coefficient to a few percent. For the systems studied here, the Zimm time ranges from $10^3\Delta t$ to $10^6\Delta t$. Given the scaling of the computation time, it is clearly advantageous to minimize the value of $b/\Delta x$.

Results for the radius of gyration R_g and the mean end-to-end distance R_e are shown in Fig. 7. The statistical properties of the polymer chains are independent of b and T, and scale in the expected way for an excluded volume chain. The numerical values of the radius of gyration fit the scaling relation $R_g = 0.4bN^{\nu}$, with $\nu = 0.59$. This is close in absolute size to the renormalization group result for a self-avoiding random walk.[22]

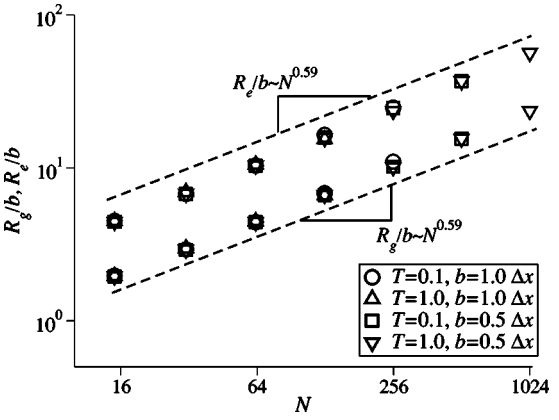

FIG. 7. End-to-end distance and radius of gyration in a periodic unit cell. The scaling of R_e (upper points) and R_g (lower points) is shown for different monomer separations, b, and temperatures, T. The dashed lines are the theoretical scalings for an excluded volume chain, with exponent $\nu = 0.59$.

The lattice-Boltzmann method simulates a finite volume rather than an unbounded domain, which has little effect on the distribution of polymer conformations but significantly reduces the diffusivity because of hydrodynamic interactions between periodic images. The box size was chosen to be a fixed multiple of the expected radius of gyration to obtain a consistent set of diffusion coefficients, as shown in Fig. 8. The raw diffusion coefficients, shown for two different box lengths, $L \sim 3.5R_g$ and $L \sim 7R_g$, scale roughly as $N^{-\nu}$, but the diffusion coefficients increase with the ratio L/R_g. The finite-size effects can be corrected by assuming that the polymer behaves hydrodynamically as a rigid sphere of radius, R_h, where

$$D = T/6\pi\eta R_h. \tag{28}$$

Then we can use the mobility of a periodic array of spheres[28] to correct for the effects of the image chains,[29]

$$D = D_L[1 + 2.84(R_h/L) + \mathcal{O}(R_h/L)^3]. \tag{29}$$

Using the relation between D and R_h [Eq. (28)], a self-consistent estimate of the diffusion coefficient in an infinite system can be obtained. Figure 8 shows that the corrected results obtained with $L \sim 3-4R_g$ are similar to those with $L \sim 6-7R_g$, and that the corrected results fall precisely on the expected scaling of diffusivity with chain length, $D \propto N^{-\nu}$. The results agree well with the renormalization group prediction for a self-avoiding random walk,[22] $D = 0.2T/\eta bN^{\nu}$. The monomer friction in these simulations was based on a hydrodynamic radius $a = b/4$, so the renormalization group prediction for the ratio of polymer to monomer diffusion coefficients is $D/D_m = 0.9N^{-\nu}$.

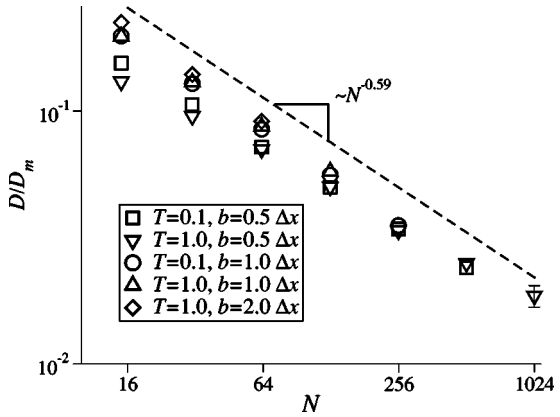

FIG. 9. Center of mass diffusion coefficient, with finite-size corrections, for different values of b and T. The length of the periodic cell $L \sim 7R_g$ in each case. The statistical uncertainties in the diffusion coefficient are smaller than the size of the symbols, except for the longest chain, $N=1024$, where they are shown explicitly.

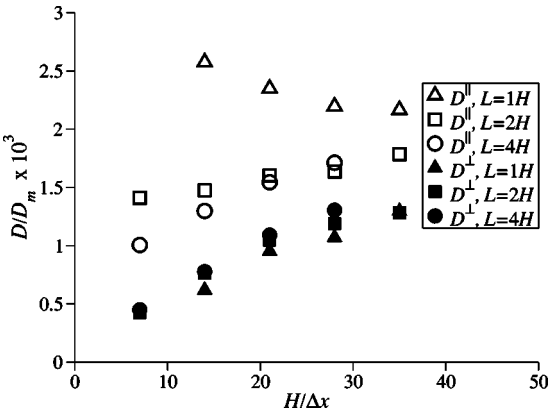

FIG. 10. Center of mass diffusion coefficients parallel ($D^{\|}$) and perpendicular ($D^{\perp}$) to the channel walls as a function of channel width H; the radius of gyration of the polymer ($N=128, b=1$) is approximately $7\Delta x$. The confined diffusion coefficients, normalized by the monomer diffusivity, are shown for a square cell, L, with various ratios of L to H.

The largest simulations in Fig. 8 extend up to 256 monomer units, and require about 5 h of computation per Zimm time. However the computational cost can be drastically reduced by either reducing the separation between neighboring monomers along the chain, b, or less dramatically, by increasing the temperature. Reducing b lowers the accuracy of the hydrodynamic interactions between nearby monomers, while increasing the temperature alters the Schmidt number and may prevent the Stokes flow field from fully developing before the monomer positions change. Diffusion coefficients for different values of b and T are shown in Fig. 9. In most simulations, we used $b=\Delta x$ as in Ahlrichs and Dünweg,[20] but for larger chains we found that smaller values of b could be used without affecting the accuracy of the calculated diffusion coefficient. For example, the diffusion coefficients of chains longer than 128 monomers obtained with $b=0.5\Delta x$ are indistinguishable from those with $b=\Delta x$. On the other hand, the smallest chains ($N<64$) require a larger value of b for a fully converged diffusion coefficient. Taken together, these results demonstrate that an accurate calculation of the diffusion coefficient is possible whenever the size of the polymer (R_g) exceeds a few grid spacings; a reasonable estimate is $R_g > 5\Delta x$. If this turns out to be true in general, hydrodynamically interacting chains can be simulated with more or less constant computational cost, regardless of chain length. Further research is needed on this point.

The scaled diffusion coefficients, D/D_m, are insensitive to temperature, except for the smallest chains ($N<64$) and the smallest mean monomer separations ($b=0.5\Delta x$). In these cases ($N<64, b=0.5\Delta x, T=1$), the polymer diffusion coefficient exceeds $0.005\Delta x^2/\Delta t$ and is not small in comparison with the kinematic viscosity of the fluid $\eta/\rho=0.167\Delta x^2/\Delta t$. Experimentally Sc typically lies in the range 10^3–10^5, but the simulation results show that a Schmidt number $\mathrm{Sc}>30$ is sufficient for an accurate measure of the diffusion coefficient. This restriction is almost invariably satisfied in our simulations, because of the large difference in diffusive time scales of the monomer and polymer.

D. Polymer diffusion in a channel

Unlike Brownian dynamics, where external boundaries present a serious complication, the lattice-Boltzmann model can simulate the dynamics of confined polymers at no additional cost. Here we consider a channel bounded in the y-direction by planar walls separated by a distance H, with periodic boundary conditions in the x and z-directions; much more complicated shapes can be implemented without difficulty. The monomer units have an additional excluded volume interaction with the wall, but the hydrodynamic calculation is unchanged. The method automatically takes account of the increased friction of a monomer near a wall[30] and the additional hydrodynamic interactions between pairs of monomers in the vicinity of the wall.[31] The simulations in the confined geometry were run for comparable times to the bulk simulations, which typically corresponds to 40–120 channel diffusion times, $t_H=H^2/4D$. However, for the weakest confinement, $H/R_g>10$, the run time was of the order of $10t_H$.

The diffusion coefficient for a confined polymer ($N=128$, $b=1$, and $T=1$) is shown in Fig. 10 for a range of channel widths $R_g<H<5R_g$, where R_g is again the radius of gyration in free solution. The diffusion coefficient in the perpendicular direction is measured at the peak in the rate of growth of the mean-square displacement, after sufficient time has elapsed for the development of the hydrodynamic interactions, but before a significant displacement of the monomers has occurred. The no-slip boundaries screen the hydrodynamic interactions in the direction parallel to the confining walls over distances greater than H. Therefore, the dependence of the diffusion coefficient on the lateral dimensions L of the cell is smaller than in the fully periodic case. In general the data show that the diffusion coefficient perpendicular to the wall, $D^{\perp}$, is independent of the area of the unit cell whenever $L>2H$. The in-plane component of the diffusivity $D^{\|}$ is more sensitive to aspect ratio than the perpendicular diffusivity, requiring $L>4H$ for convergent results. Moreover, when $H \sim R_g$ there is an additional constraint, $L>4R_g$, in order to prevent direct interactions between chains that are flattened by the narrow channel.

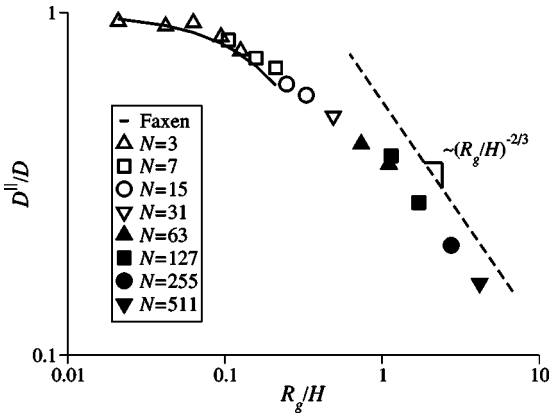

FIG. 11. Center of mass diffusion coefficient for a confined polymer relative to the unconfined diffusivity, $D^{\parallel}/D$. The solid line indicates the Faxen correction (Ref. 30) for weak confinement, assuming the polymer lies in the center of the channel. The dashed line is the theoretical $(R_g/H)^{-2/3}$ scaling (Ref. 32). The aspect ratio of the cell, L/H, was set to 4 or $4R_g/H$, whichever was larger.

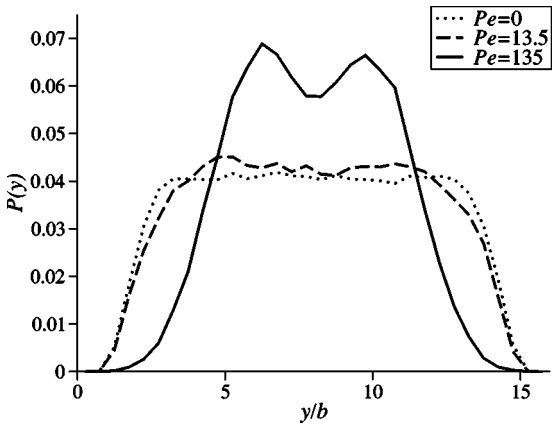

FIG. 12. Monomer distribution for a chain composed of $N=16$ monomers ($b=1, R_g \approx 2\Delta x$) in a confined channel, $H=16\Delta x$, at different flow rates: Pe=0 (dotted), 13.5 (dashed), and 135 (solid).

The scaling of the parallel diffusion coefficient in a confined geometry is shown in Fig. 11 for a range of confinement ratios, R_g/H. The diffusion coefficient $D^{\parallel}/D$ of a weakly confined polymer, $R_g/H \ll 1$, is consistent with the reduction in mobility of a confined sphere[30] of radius R_h. In tighter confinement, $R_g/H > 1$, there is a transition to a power-law decay, which is consistent with the predictions of scaling theory,[32] $D^{\parallel}/D \propto (R_g/H)^{-2/3}$. On the other hand Brownian dynamics simulations in a square channel[4] suggest an exponent closer to $-1/2$. This result is supported by numerical mean-field calculations,[33] which indicate that the asymptotic scaling is not reached in two-dimensional confinement until extremely long chain lengths, in excess of 10^6 segments. However the confinement in a slit is less severe than in a tube, and a mean-field calculation would be useful to confirm that scaling theory applies to much shorter chains in one-dimensional confinement.

E. Polymer distribution in a channel flow

The center-of-mass distribution of a weakly confined polymer, $H \approx 8R_g$, in a pressure-driven flow has been calculated for a variety flow rates. The Peclet number characterizing the flow, $\mathrm{Pe} = \gamma R_g^2/D$, is based on the mean shear rate $\gamma = \nabla p H/4\eta$, the radius of gyration and the polymer diffusivity. The center-of-mass distribution in the channel is shown in Fig. 12 for Peclet numbers Pe=0, 13.5, and 135, using the unconfined values for the radius of gyration, R_g, and diffusion coefficient, D. From the Zimm model for the longest relaxation time,[34] $\tau_1 = 0.9\eta b^3 N^{3\nu}/T$, we estimate that the Weissenberg number is about 10% larger than the Peclet number. The two lowest Peclet numbers were obtained at a temperature $T=0.5$, while the highest Peclet number was run at a temperature $T=0.05$. Each calculation was run for a total of 10^8 time steps, while the channel diffusion time $H^2/4D$ was approximately 19 000 steps at the higher temperature and 190 000 steps at the lower one.

The maximum flow velocity is restricted by the condition $u_{\max}/c_s < 0.3$, which is necessary for the lattice-Boltzmann model to approximate an incompressible flow. In practice this means that the maximum shear rate is limited and declines with increasing channel width. Thus to obtain higher Peclet numbers (or Weissenberg numbers) the polymer diffusivity must be reduced. In the relatively narrow channels studied here this restriction was not serious, but the computational cost increases rapidly with larger channels. We are investigating ways of introducing a base flow field into the lattice-Boltzmann model,[35] and then simulating the difference in velocity from the imposed flow field. In this case the incompressibility restriction will apply only to the difference field, removing the limitation on flow velocity.

At equilibrium (Pe=0), a uniform distribution exists across most of the channel width, with a depletion layer near each wall of order $R_g \sim 2b$. At low flow rates (Pe=13.5), the thickness of the depletion layer increases slightly. This weak migration is due to the combined effect of hydrodynamic interactions between the pairs of monomers and hydrodynamic interactions between a monomer and a wall;[2] neglecting either one of these interactions leads to a qualitatively different result. In the absence of hydrodynamic interactions, the depletion layer thickness decreases with increasing flow strength, due to stretching of the polymer chain by the high shear rate near the wall, enabling the center of mass to access regions closer to the boundary.

At higher flow rates (Pe=135), there is a strong overall migration of the polymer chain towards the center of the channel, but there is a slightly lower concentration at the center of the channel than in the neighboring regions. These observations agree qualitatively with Brownian dynamics simulations of polymer flow in a square channel.[2] The distribution of the center of mass arises from a balance of the Brownian drift towards a uniform distribution and the hydrodynamic migration of a flexible polymer away from the walls. The slight dip at the centerline is presumably due to a coupling between the polymer configuration and the cross-channel diffusion coefficient. At the center, the polymer experiences relatively little shear and will therefore exist in a less extended state than a polymer located slightly off the centerline. The more extended polymer has a lower diffusivity perpendicular to the walls, therefore the higher diffusivity at the center creates a slight deficit for the distribution of polymer at the center.

IV. CONCLUSIONS

We have implemented and tested an inertial simulation of the dynamics of a single polymer chain in solution. The method is based on a lattice-Boltzmann model of a thermally fluctuating fluid and a point-particle representation of the interaction between the polymer chain and the fluid. We tested the method using known results for the dissipative and fluctuating dynamics of one and two-particle systems, and found that the long-range Oseen level hydrodynamic interactions were reproduced quantitatively. Surprisingly, the time step is comparable to typical Brownian dynamics simulations. This fact, together with the more favorable scaling of the computational time with respect to the size of the chain, has enabled us to perform dynamical simulations of longer chains than has previously been possible. We obtained the expected scaling for the diffusion constant in an unconfined system for chain lengths up to $N=1024$ monomers. The results suggest that a coarse graining of the hydrodynamic interactions is possible for very long chains, keeping the radius of gyration at a fixed number of grid points of the underlying fluid. In this case, the computational cost of calculating hydrodynamic interactions is independent of chain length. The method can be readily extended to complex confinement geometries, with or without an imposed flow field. Our results for confined channels are qualitatively consistent with Brownian dynamics simulations in a square duct.[2,4] Although all these tests have been for a single chain, multichain simulations are straightforward and require minimal additional computation if the system volume remains fixed.

ACKNOWLEDGMENT

This work was partially supported by the National Science Foundation through a CAREER Award (CTS-0348205).

APPENDIX: DISCRETE LANGEVIN EQUATION

Numerical simulations show that the mean kinetic energy of a single monomer is different from what would be expected from the level of the stress fluctuations in the fluid (Fig. 3). Nevertheless, the fluctuation-dissipation relation between the effective friction and diffusion coefficients holds within statistical errors (Fig. 1). It has been shown[10] that fluctuations in a discrete system can be different from those in continuous systems [cf. Eqs. (11) and (12)], and in order to understand why deviations from classical equipartition do not affect the long-time dynamics, we here examine a simple model with constant friction. The dynamics are described by the classical Langevin equation,

$$m\frac{dU}{dt} = -\xi U + R(t), \tag{A1}$$

with a variance in the random force $\langle R(t)R(t')\rangle = 2\xi T\delta(t-t')$. With this choice of random force, Eq. (A1) satisfies both the Stokes–Einstein relation $D=T/\xi$ and equipartition $m\langle U^2\rangle = T$. The real situation is more complex,[25,36] with a time-dependent friction coefficient due to the temporal and spatial development of the hydrodynamic flow field. Nevertheless, this simple model is sufficient to illustrate the deviations in mean kinetic energy from classical equipartition.

The discrete equivalent of Eq. (A1) can be written as

$$U(t+\Delta t) = (1-\Omega)U(t) + \Delta U(t), \tag{A2}$$

where $\Omega = \xi\Delta t/m$ and $\langle \Delta U(t)\Delta U(t')\rangle = (2\Omega T/m)\delta_{t,t'}$. The level of fluctuation in the random velocity, ΔU, has been calculated by integrating the random force over the time step Δt,[37]

$$\Delta U(t) = \frac{1}{m}\int_t^{t+\Delta t} R(t')dt'. \tag{A3}$$

After n time steps, Eq. (A2) has the solution

$$U(t+n\Delta t) = (1-\Omega)^n U(t) + \sum_{k=0}^{n-1} \Delta U(t+k\Delta t) \times (1-\Omega)^{(n-1-k)}, \tag{A4}$$

with the usual stability condition $\Omega<2$. At long times, $n \gg 1$, the particle temperature is related to the fluid temperature by

$$m\langle U^2\rangle = 2T\Omega\sum_{k=0}^{\infty}[(1-\Omega)^2]^k = \frac{T}{1-\Omega/2}, \tag{A5}$$

and violates the classical equipartition of energy. On the other hand, the diffusion coefficient, which can be calculated from the discrete equivalent of the Green–Kubo relation

$$D = \frac{\Delta t}{2}\langle U(0)U(0)\rangle + \Delta t\sum_{n=1}^{\infty}\langle U(n\Delta t)U(0)\rangle = \frac{T}{\xi}, \tag{A6}$$

satisfies the Stokes–Einstein relation. Thus we recover the correct long-time diffusive behavior, despite the discrete time step, whereas the kinetic energy has an additional factor $(1-\Omega/2)^{-1}$. An accurate equipartition of energy requires that $\Omega \ll 1$, which in our context means that the mass of the monomer must be large. However, numerical calculations with $\Omega<0.5$ show that the diffusive behavior of interacting particles is unaffected by violations of equipartition.

An implicit update of Eq. (A1),

$$U(t+\Delta t) = U(t) - \Omega U(t+\Delta t) + \Delta U(t), \tag{A7}$$

is often used to circumvent the stability constraint $\Omega<2$ on the explicit solution [Eq. (A2)]. It is straightforward to show that the Stokes–Einstein relation $D=T/\xi$ is again satisfied, but in this case the mean kinetic energy is given by

$$m\langle U^2\rangle = \frac{T}{1+\Omega/2}. \tag{A8}$$

The comparison of Eqs. (A5) and (A8) with the numerical simulations is shown in Fig. 3. It can be seen that the simplified model presented here, which neglects the time-dependence of the hydrodynamic interactions, still predicts the deviations from equipartition quantitatively.

[1] M. Fixman, Macromolecules **19**, 1204 (1986).
[2] R. M. Jendrejack, D. C. Schwartz, J. J. de Pablo, and M. D. Graham, J. Chem. Phys. **120**, 2513 (2004).
[3] R. M. Jendrejack, M. Graham, and J. dePablo, J. Chem. Phys. **113**, 2894 (2000).

[4]R. M. Jendrejack, M. Graham, and J. dePablo, J. Chem. Phys. **119**, 1165 (2003).
[5]N. J. Woo, E. Shaqfeh, and B. Khomami, J. Rheol. **48**, 281 (2004).
[6]N. J. Woo, E. Shaqfeh, and B. Khomami, J. Rheol. **48**, 299 (2004).
[7]C.-C. Hsieh and R. G. Larson, J. Rheol. **48**, 995 (2004).
[8]R. Prabhakar, J. R. Prakesh, and T. Sridhar, J. Rheol. **48**, 1251 (2004).
[9]A. J. C. Ladd, J. Fluid Mech. **271**, 285 (1994).
[10]A. J. C. Ladd and R. Verberg, J. Stat. Phys. **104**, 1191 (2001).
[11]A. J. C. Ladd, J. Fluid Mech. **271**, 311 (1994).
[12]A. J. C. Ladd, Phys. Rev. Lett. **70**, 1339 (1993).
[13]A. J. C. Ladd, H. Gang, J. X. Zhu, and D. A. Weitz, Phys. Rev. Lett. **74**, 318 (1995).
[14]A. J. C. Ladd, Phys. Rev. Lett. **76**, 1392 (1996).
[15]A. J. C. Ladd, Phys. Rev. Lett. **88**, 048301 (2002).
[16]C. K. Aidun, Y. N. Lu, and E. Ding, J. Fluid Mech. **373**, 287 (1998).
[17]F. M. Auzerais, J. Dunsmuir, B. B. Ferréol *et al.*, Geophys. Res. Lett. **23**, 705 (1996).
[18]N. S. Martys and H. Chen, Phys. Rev. E **53**, 743 (1996).
[19]B. Manz, L. F. Gladden, and P. B. Warren, AIChE J. **45**, 1845 (1999).
[20]P. Ahlrichs and B. Dünweg, J. Chem. Phys. **111**, 8225 (1999).
[21]P. Ahlrichs, R. Everaers, and B. Dünweg, Phys. Rev. E **64**, 040501(R) (2001).
[22]Y. Oono and M. Kohmoto, J. Chem. Phys. **78**, 520 (1983).
[23]J. F. Marko and E. D. Siggia, Macromolecules **28**, 8759 (1995).
[24]U. Frisch, D. d'Humières, B. Hasslacher *et al.*, Complex Syst. **1**, 649 (1987).
[25]L. D. Landau and E. M. Lifshitz, *Fluid Mechanics* (Addison-Wesley, London, 1959).
[26]D. L. Ermak and J. A. McCammon, J. Chem. Phys. **69**, 1352 (1978).
[27]X. Fan, N. Phan-Thien, N. T. Yong, X. Wu, and D. Xu, Phys. Fluids **15**, 11 (2003).
[28]H. Hasimoto, J. Fluid Mech. **5**, 317 (1959).
[29]A. J. C. Ladd, J. Chem. Phys. **93**, 3484 (1990).
[30]J. Happel and H. Brenner, *Low-Reynolds Number Hydrodynamics* (Martinus Nijhoff, Dordrecht, 1986).
[31]T. M. Squires and M. P. Brenner, Phys. Rev. Lett. **85**, 4976 (2000).
[32]F. Brochard and P. G. de Gennes, J. Chem. Phys. **67**, 52 (1977).
[33]J. L. Harden and M. Doi, J. Phys. Chem. **96**, 4046 (1992).
[34]M. Doi and S. F. Edwards, *The Theory of Polymer Dynamics* (Oxford University Press, Oxford, 1986).
[35]A. J. Wagner and I. Pagonabarraga, J. Stat. Phys. **107**, 521 (2002).
[36]E. H. Hauge and A. Martin-Löf, J. Stat. Phys. **7**, 259 (1973).
[37]H. C. Öttinger, *Stochastic Processes in Polymeric Fluids* (Springer-Verlag, Berlin, 1996).